International Journal of GEOMATE, Oct., 2024 Vol.27, Issue 122, pp.115-123
ISSN: 2186-2982 (P), 2186-2990 (O), Japan, DOI: https://doi.org/10.21660/2024.122.g13225
Geotechnique, Construction Materials and Environment

CHANGES IN THE NETWORK PROPERTY OF PORES DUE TO SOIL AGGREGATE FORMATION

Goto Atsushi[1], Takeuchi Junichiro[1*], Takeuchi Yuto[1] and Fujihara Masayuki[1]

[1]Graduate School of Agriculture, Kyoto University, Japan

*Corresponding Author, Received: 10 July 2023, Revised: 30 July 2024, Accepted: 25 Sep. 2024

ABSTRACT: Soil aggregates are clumps of soil particles bound to each other through organic matter. Soil with aggregates has favorable features for crop cultivation, such as adequate water retention and filtration. This feature was clarified from the perspective of the network formed by pores. The connectivity of pore networks in soil was investigated in this study using virtually generated porous media with and without aggregates. The connectivity for drainability was evaluated using the percolation probability (PP), which is represented as a curve of the ratio of the largest subnetwork formed by pores that are larger than a certain value as the value decreases from the maximum to the minimum pore size. Compared with the PP of porous media without aggregates, PP with aggregates has a smaller percolation threshold, which is the point at which PP rises sharply, indicating that soil with aggregates has high drainability. Furthermore, PP without aggregates asymptotically approached the diagonal, whereas PP with aggregates left the diagonal halfway and approached again. This demonstrates that the aggregates contain loosely isolated subnetworks and that the water retained in the aggregates is difficult to drain once the aggregates are filled with water. These findings enhanced our understanding of the water retention property of soils with aggregates.

Keywords: Soil aggregates, Pore-network, Percolation probability, Percolation threshold, Water retention

1. INTRODUCTION

Soil is a vital component of ecosystems across the globe. One of the most important functions of soil is centered around retaining air, water, and nutrients and serving them to plants.

The abovementioned function of soil is largely shaped by soil aggregates, which are clumps of soil particles bound to each other by organic matter. Soil aggregate makes large pores between aggregates and small ones in aggregate, and the variety of pore size influences the function of soil. The emission of CO_2 and CH_4 from soil aggregates has been shown to be shaped by their sizes [1]. Another study showed that soil aggregates explained 68.4% of the variation in the soil bacterial community [2]. Moreover, Gao *et al.* [3] showed large aggregates in soils under three types of tillage treatment contained higher soil organic carbon.

Pores in the soil can be investigated using microtomography, and the relationship between the characteristics of the pores of soil aggregates can be studied through the lens of the primary functions of soil. Mangalassery *et al.* [1] showed that porosity and pore size in aggregates significantly affect fluxes of greenhouse gases such as CO_2 and CH_4. Factors that shape the pore structure of aggregates have also been investigated. For example, Zhou *et al.* [4] and Zhao *et al.* [5] revealed that revegetation increases porosity while decreasing the number of pores.

Most studies on pore structure in aggregates have quantified characteristics of the structure using the distribution of pore size; this approach does not allow for the spatial distribution of pores. Additionally, some studies have examined the spatial dynamics of pores. For example, Wang *et al.* [6] and Gao *et al.* [7] divided aggregate into two or three layers so that the volume of each layer is the same and compared the properties of the pore in the inner and outer layers. Peth *et al.* [8] visualized channels of pores in aggregates and quantified properties of pores and channels. However, these studies did not illuminate the relationship between pore size and the spatial connection of pores.

Therefore, this study aims to investigate spatial characteristics of void space in aggregates. In previous studies, virtual porous media with aggregates composed of uniformly sized spherical particles were investigated using Moran's *I* and percolation theory using the pore network model. In this study, the spatial distribution, connectivity, and hydraulics underlying the drainage of virtual porous media composed of particles of varying sizes were investigated. We expect Moran's *I* and percolation threshold to be larger and lower than those revealed in a previous study, respectively [9].

2. RESEARCH SIGNIFICANCE

This study enhances the understanding of soil aggregate characteristics from the perspective of networks. In this study, the percolation probability

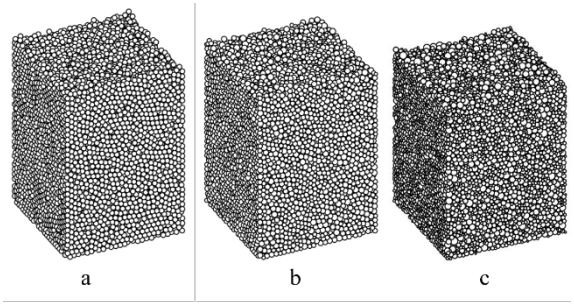

Fig. 1 Virtual porous media without aggregates

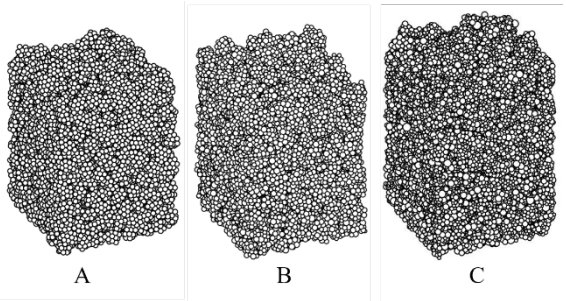

Fig. 2 Virtual porous media with aggregates

(PP) and invaded percolation probability (IPP), which are connectivity feature values of a pore-network present in porous media were investigated. The results suggest that in the aggregates, relatively large pores were surrounded by small pores. This confers unique characteristics to the soil with aggregates, such as higher water retention.

3. METHOD

3.1 Generation of Porous Media and Extraction of Pore-network

Virtual porous media and pore-network models of their void spaces were created to investigate the pore connectivity and hydraulic properties of porous media. Virtual porous media were generated by randomly packing spherical particles using the discrete element method. Cohesive forces were introduced between the particles according to the JKR (Johnson-Kendall-Roberts) model to form an aggregate structure [10, 11] although this way mightn't perfectly imitate real aggregate structure because particles can overlap due to characteristic of discrete element method. After the porous media are created, pore-network models are extracted using SNOW [12], an application that uses the watershed algorithm [13]. A pore-network model represents void spaces connected to each other in a porous medium using pore bodies (PBs), which are relatively large spherical pores, and pore throats (PTs), which are relatively small cylindrical pores that connect two PBs. Pore network model simplify void of porous media and can be used to study complex multiphase flow problems in large domains, such as entire catalyst pellets, electrodes, and paper [12].

In this research, six cases of porous media, namely a, b, c, A, B, and C, were prepared. These cases were divided into three categories based on the particles comprising the media. Cases A and a were composed of particles with a diameter of 0.2 mm. Cases B and b were composed of particles with diameters that followed the normal distribution whose average and standard deviation are 0.2 mm and 0.027 mm, respectively, and Cases C and c are particles following a normal distribution whose average and standard deviation were 0.2 and 0.053 mm. Lower case letters (Fig. 1) refer to media without an aggregate structure, and capital letters refer to media with an aggregate structure (Fig. 2) and a diameter of 0.8 mm. In all cases, virtual porous media were prepared by packing spherical particles randomly into a rectangular parallel-piped container whose base is 53.3 mm square and then cutting a 33.3 mm cube from it to avoid the effects of the walls. Three porous media were prepared for each case to ensure adequate volume. Pore-network models were extracted from the voxel data of the cut-out media with a resolution of 700^3, where voids were represented as 0 and substrates as 1. The container size and resolution were determined according to a previous study [9].

3.2 Spatial Autocorrelation of PB Size

Moran's *I* was used to evaluate the spatial distribution of pores. Moran's *I* is an index of the spatial autocorrelation of a target attribute inside an entire system and is represented by Eq. (1) [14]:

$$\boldsymbol{I} = \frac{\boldsymbol{n}\sum_{i=1}^{n}\sum_{j=1}^{n}\boldsymbol{w_{ij}}(\boldsymbol{x_i}-\overline{\boldsymbol{x}})(\boldsymbol{x_j}-\overline{\boldsymbol{x}})}{\boldsymbol{S_0}\sum_{i=1}^{n}(\boldsymbol{x_i}-\overline{\boldsymbol{x}})^2}, \quad (1)$$

$$\overline{\boldsymbol{x}} = \frac{1}{\boldsymbol{n}}\sum_{i=1}^{n}\boldsymbol{x_i}, \quad (2)$$

$$\boldsymbol{S_0} = \sum_{i=1}^{n}\sum_{j=1}^{n}\boldsymbol{w_{ij}}, \quad (3)$$

where $\boldsymbol{n}$, $\boldsymbol{x_i}$,and $\boldsymbol{w_{ij}}$ are the number of data points, value of the target attribute (pore diameter), and component of the spatial weight matrix, respectively. Moran's *I* ranges from −1 to 1. Spatial variables have a positive (or negative) autocorrelation if their Moran's *I* is positive (or negative), and a large (or small) absolute value of Moran's *I* implies that the autocorrelation is strong (or weak). The significance of Moran's *I* was verified using a statistical test under the null

hypothesis of no spatial autocorrelation, where Moran's *I* has asymptotic normality.

The spatial distribution of the PB diameter was investigated in this study. The components of the weight matrix are 1 if two PBs are adjacent; otherwise, 0 is considered.

3.3 Percolation Probability

The PP was calculated to evaluate the connectivity of the pore-network. The percolation probability is the likelihood that a pore is included in the largest subnetwork of open pores. If the network is finite, it is evaluated by the ratio of the largest cluster of open pores to all the pores. In the drainage process, "open" pores are pores through which air can enter when a water-air interface is present at the entrance of the pore. A scatter plot between PP (vertical axis) and the proportion of open pores (horizontal axis) was used to examine the percolation capacity. Generally, PP increases sharply when the proportion of open pores reaches a certain level. This ratio is known as the percolation threshold. When the proportion of open pores reaches the percolation threshold, the largest cluster of open pores spreads throughout the pore-network.

In this study, the drainage process in porous media was investigated, and both PB and PT were considered sites of percolation according to Takeuchi and Fujihara [15].

3.4 Invasion Percolation

The drainage of a porous medium filled with water was evaluated by applying the invasion percolation method originally proposed by Wilkinson and Willemsen [16] to the pore-network model.

To understand the drainage process of porous media, it is necessary to detect the pores containing both PB and PT that are potentially invadable. If $\boldsymbol{I_{AE} > 0}$ in Eq. (4), the pores are potentially invadable [15].

$$\boldsymbol{I_{AE} = p_c - p_{AE}}, \quad (\mathbf{4})$$

$$\boldsymbol{p_c = p_{air} - p_{water}}, \quad (\mathbf{5})$$

$$\boldsymbol{p_{AE} = \frac{P\sigma \cos\theta}{A}}, \quad (\mathbf{6})$$

$$\boldsymbol{p_{water} = p_{btm} - \Delta z}, \quad (\mathbf{7})$$

where $\boldsymbol{p_c}$, $\boldsymbol{p_{air}}$, $\boldsymbol{p_{water}}$, and $\boldsymbol{p_{AE}}$ are the capillary, atmospheric, water, and air entry pressures, respectively. $\boldsymbol{P}$, $\boldsymbol{A}$, $\boldsymbol{\sigma}$, $\boldsymbol{\theta}$, $\boldsymbol{p_{btm}}$, $\boldsymbol{\Delta z}$ represent the perimeter of a cross sectional area, the cross-sectional area, the surface tension of water, the contact angle between water and a soil particle, the matric potential of the bottom of a porous medium, and the height of a pore from the bottom of a porous medium, respectively. The intrusion of air into porous media is determined by the following processes [17, 18].

1. All PBs and PTs are filled with water, and a certain water pressure is imposed on the bottom of a pore-network.
2. All PBs and PTs that defend against air intrusion and satisfy the accessibility rule are listed and sorted in descending order based on the invadability value.
3. Among the listed PBs and PTs, the interfaces of the top N^{IP} were moved simultaneously (the state in the pores was changed from water to air) if the invadability value was positive.
4. Processes 2 and 3 are iterated until no state change occurs, and saturation of the pore-network is calculated when a steady state is achieved.

The bottom and upper surfaces of the porous medium were connected to the water and air pools, respectively. Water and air cannot pass through other surfaces. In this study, two scenarios were simulated. In the first pattern, N^{IP} was set to 10 and after a steady state was achieved, the state was used as the initial condition, and the calculation was iterated with a decreased bottom pressure. In the second pattern, N^{IP} was set to 10,000, a value large enough to account for all invadable pores in pore-network, and after a steady state was achieved, the calculation was iterated with decreased bottom pressure using the conditions of process 1, in which all PBs and PTs were filled with water. The former was referred to as Pattern 1 and the latter as Pattern 2. Pattern 1 corresponds to relatively small capillary number and Pattern 2 does to relatively large capillary number [17]. The matrix potential at the bottom changed from 20 cm H_2O to −220 cm H_2O in both patterns.

3.5 Water Retention Curve (WRC) and Invaded Percolation Probability (IPP)

The water retention curve (WRC) and invaded percolation probability (IPP) were used to evaluate the drainage process. The WRC shows the relationship between the matrix potential at the bottom of the porous medium and saturation. The IPP is the ratio of the number of pores in the largest cluster of invaded pores to the total number of pores. IPP is also plotted in a scatter diagram, whose horizontal axis indicates the proportion of open pores, and the vertical axis represents the proportion of IPP in the same manner as PP [19].

4. RESULTS AND DISCUSSION

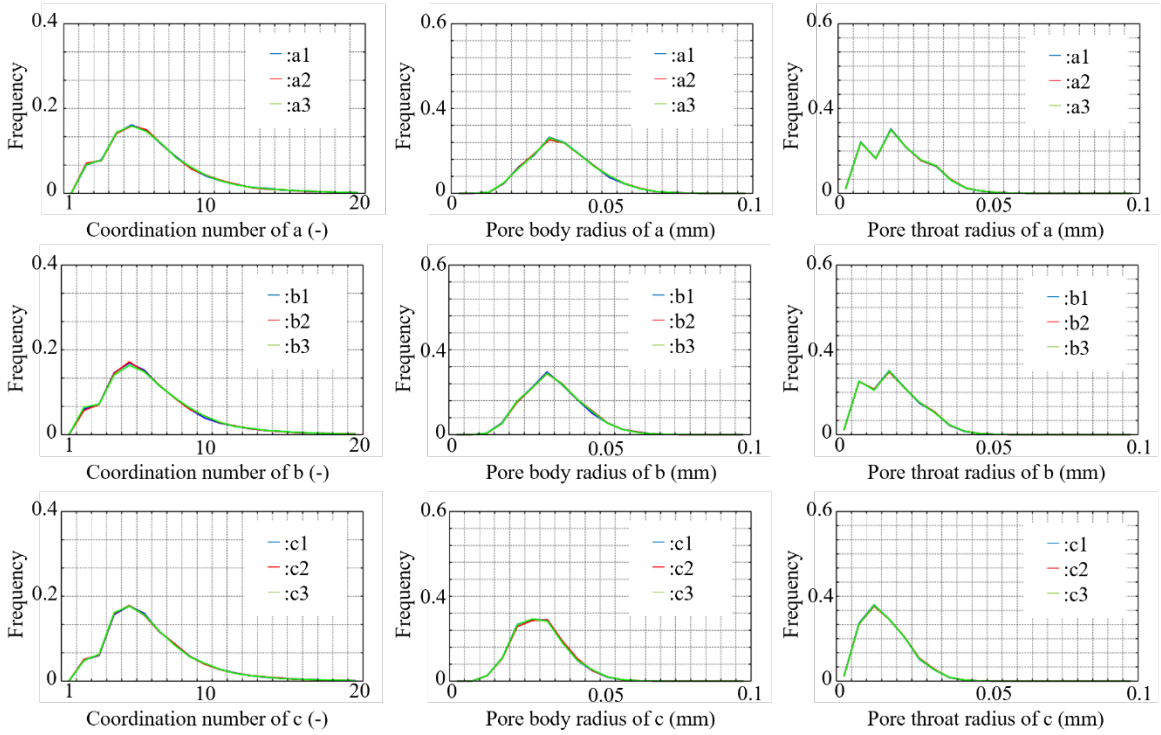

Fig. 3 Coordination number, pore body (PB) radius and pore throat (PT) radius of pore-network models without aggregates

a: composed of particles with a diameter of 0.2 mm, b: composed of particles with diameters that followed the normal distribution whose average and standard deviation are 0.2 mm and 0.027 mm, respectively, c: composed of particles with diameters that followed the normal distribution whose average and standard deviation are 0.2 mm and 0.053 mm

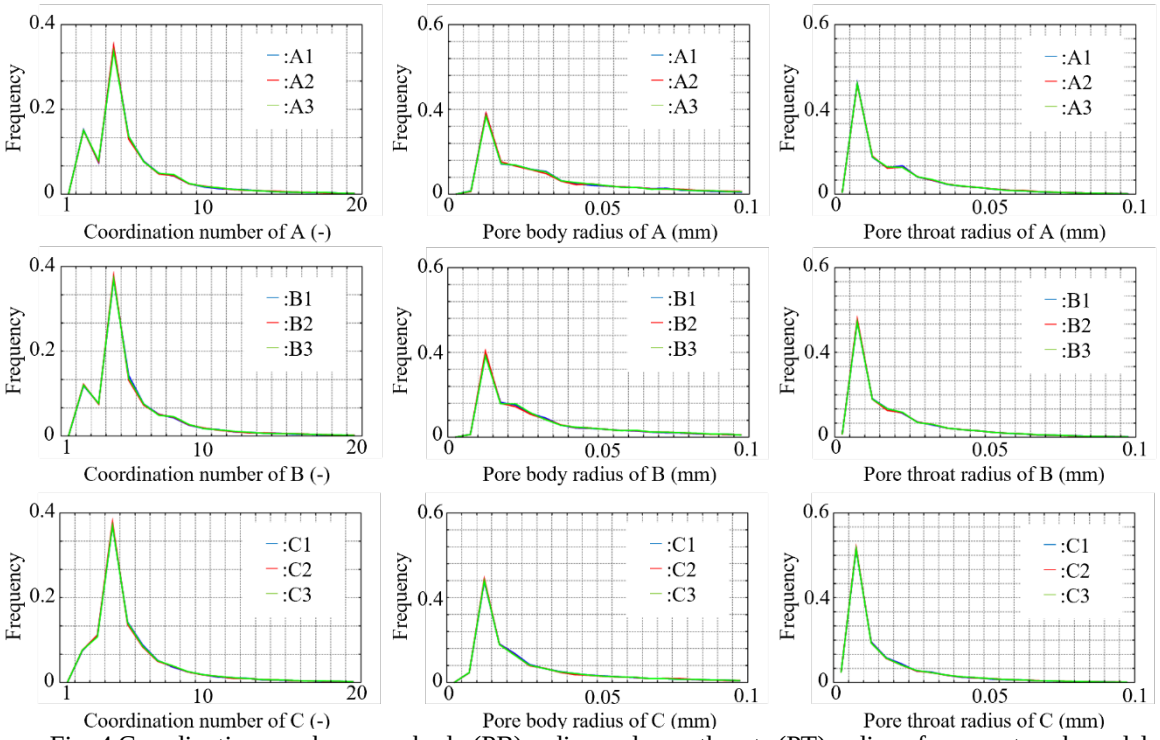

Fig. 4 Coordination number, pore body (PB) radius and pore throats (PT) radius of pore-network models with aggregates

A: composed of particles with a diameter of 0.2 mm, B: composed of particles with diameters that followed the normal distribution whose average and standard deviation are 0.2 mm and 0.027 mm, respectively, C: composed of particles with diameters that followed the normal distribution whose average and standard deviation are 0.2 mm and 0.053 mm

4.1 Histograms of Pore Properties

Figures 3 and 4 show the histograms of the coordination number, or the number of PTs connected to one PB, and the radii of the PBs and PTs for each case. In all histograms, the results of the three porous media were comparable and suggest that all porous media have adequate volumes to evaluate the WRCs, PPs, and IPPs. The figures show that the frequency of large pores (PBs and PTs) increases in the porous media with aggregates compared to the porous media without aggregates because of the voids between the aggregates.

4.2 Spatial Autocorrelation of PB Size

The Moran's *I* and Z scores for each sample are shown in Table 1. The *Z* scores in each sample are sufficiently large, which indicates that the *p*-values are approximately zero and that the obtained Moran's *I* of the PB-size spatial distribution in porous media is significant in all cases. All values of Moran's *I* are positive, which means that the spatial distribution of PB size has a positive spatial autocorrelation. The Moran's *I* of porous media with aggregates was greater than that of media without aggregates. This indicates that there are larger pore clusters whose pore sizes are similar in porous media with aggregates compared to those in porous media without aggregates. Clusters with similar pore sizes were formed in the aggregates. Takeuchi *et al.* [9] showed that porous media consisting of uniform, aggregated particles have a greater Moran's I than porous media without aggregates. Additionally, it has been shown that porous media composed of particles (aggregated) of various sizes also have a greater Moran's *I*. Ref. [6] examined intra-aggregate pore characteristics using X-ray computed microtomography and found that large pores tended to prevail in the aggregate interiors while medium size pores were more abundant in the aggregate exteriors. It may be possible that virtual porous media with aggregate structure had this tendency, and similar-size pores became likely to neighbor to each other, which caused high Moran' I.

4.3 WRC

Figures 5-8 depict the WRC, which revealed that the air-entry pressure of the porous media with aggregates was lower than that of the porous media without aggregates because of the larger pores between the aggregates. The residual water content in porous media with and without aggregates is about 40% and 50% in pattern 1 and 20% and 12% in pattern 2, respectively.

Table 1 Moran's *I* of PB size

Samples	Moran's *I*	*Z*-score
a1	0.248	68.0
a2	0.259	70.7
a3	0.260	71.1
Average	0.256	96.9
b1	0.256	75.0
b2	0.253	73.7
b3	0.262	77.1
Average	0.257	75.3
c1	0.287	98.4
c2	0.273	92.4
c3	0.294	99.8
Average	0.285	96.9
A1	0.817	169.6
A2	0.819	172.6
A3	0.808	167.8
Average	0.815	170.0
B1	0.804	172.7
B2	0.798	171.9
B3	0.776	166.3
Average	0.793	170.3
C1	0.778	189.8
C2	0.798	190.3
C3	0.785	188.9
Average	0.787	189.7

4.4 PP and IPP

Figures 9-12 show the PP and IPP for each case, respectively. The percolation threshold in porous media with aggregate structures (Cases A, B, and C) was approximately 0.05, which was significantly lower than that in porous media without aggregate structures (Cases a, b, and c). This indicates that the pore-networks with aggregates form a sub-network of the top 5% of large pores, which spreads throughout the medium, whereas the pore-network without aggregates requires the top 35% of large pores to form such a sub-network. From the IPP graphs, it is evident that air begins to invade according to the percolation thresholds in all cases in both patterns and that water remains in 85% and 75–82% of the pores in pore-networks with and without aggregates in pattern 1 and 35% and 40% in pattern 2, respectively. It was revealed not only percolation thresholds of porous media composed of uniform size particles but also those of media composed of varying sizes of particles get lower due to formation of aggregate.

The PP of the pore-networks without aggregates approached the diagonal of the diagram as the proportion of open pores increased, whereas the PP of the pore-network with aggregates left the diagonal halfway and approached it again. This behavior is characteristic of porous media with an aggregate structure and indicates the presence of medium-sized pores that are loosely isolated from larger open pores. These dynamics were not observed in previous studies. This could be because in this study, the particles were packed in a larger container, lessening the influence of the walls.

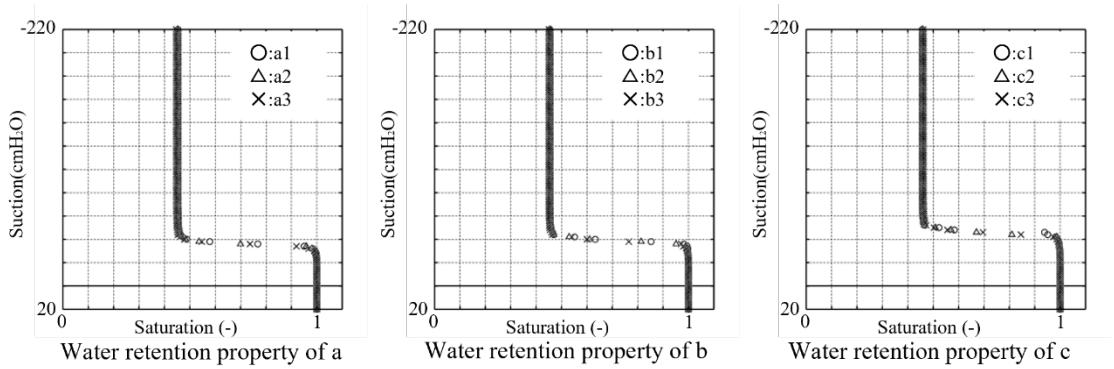

Fig. 5 Water retention curves of porous media without aggregates (Cases a, b and c: Pattern 1)

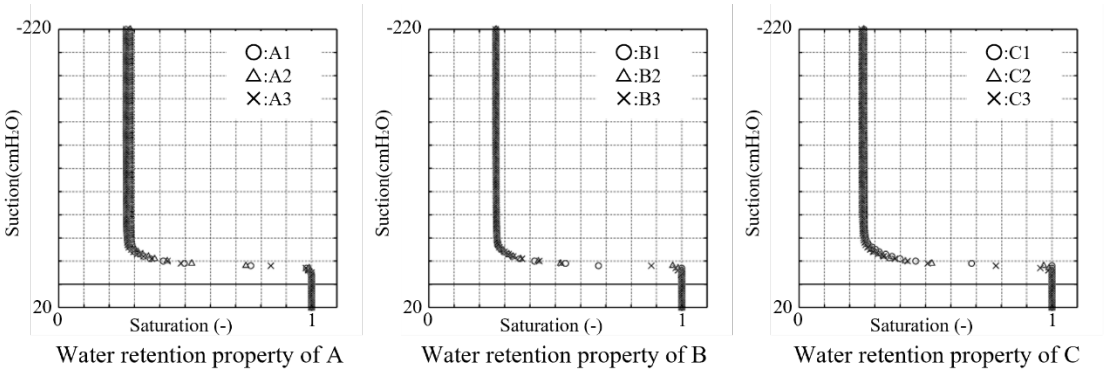

Fig. 6 Water retention curves (WRC) of porous media with aggregates (Cases A, B and C: Pattern 1)

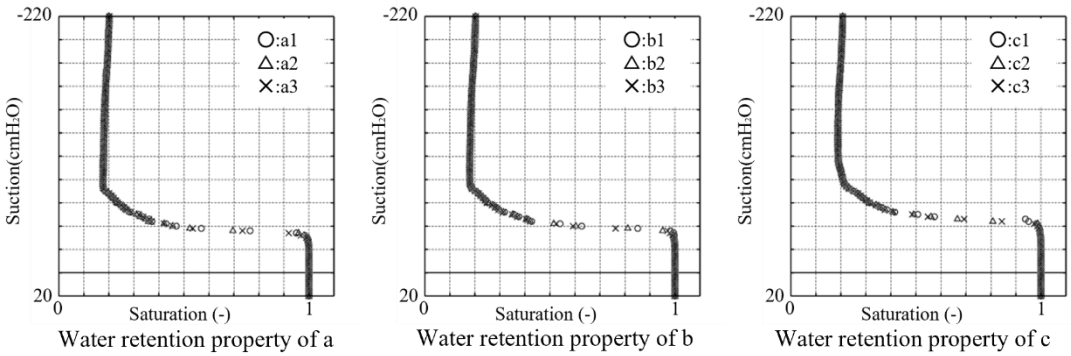

Fig. 7 Water retention curves of porous media without aggregates (Cases a, b and c: Pattern 2)

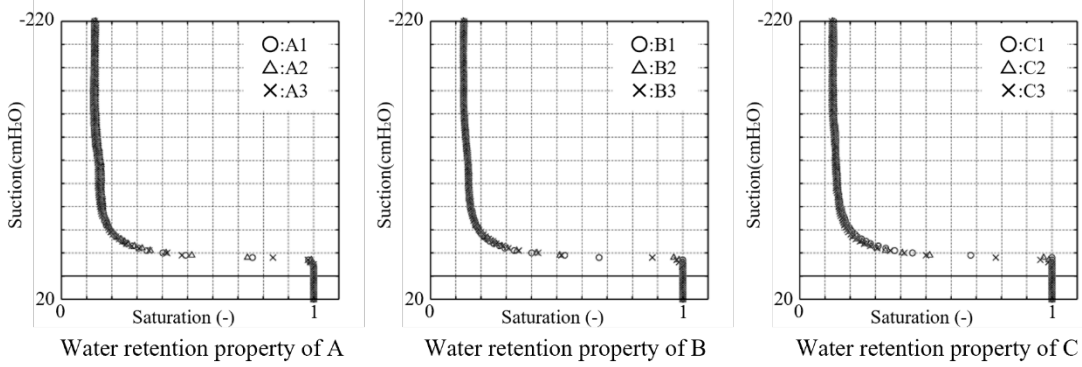

Fig. 8 Water retention curves (WRC) of porous media with aggregates (Cases A, B and C: Pattern 2)

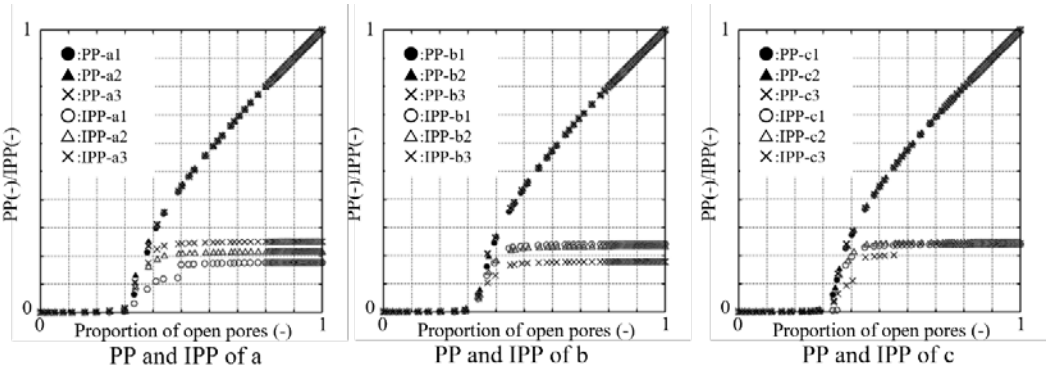

Fig. 9 Percolation probability and invaded percolation probability of porous media without aggregates (Cases a, b and c: Pattern 1)

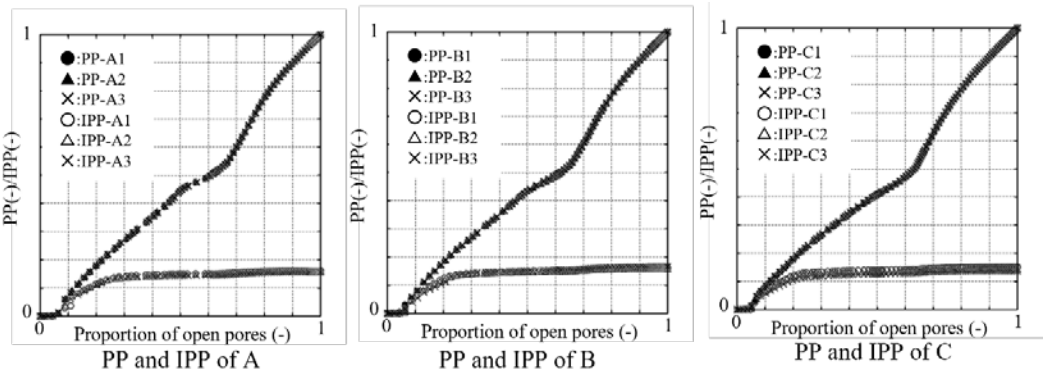

Fig. 10 Percolation probability (PP) and invaded percolation probability (IPP) of porous media with aggregates (Cases A, B and C: Pattern 1)

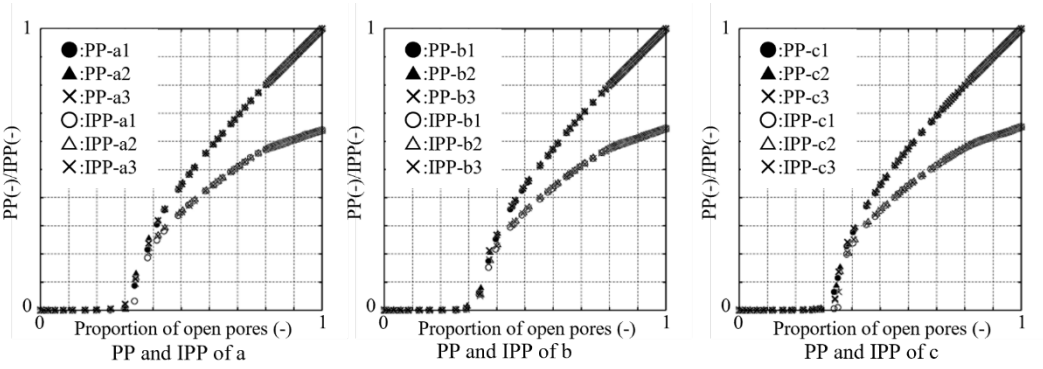

Fig. 11 Percolation probability and invaded percolation probability of porous media without aggregates (Cases a, b and c: Pattern 2)

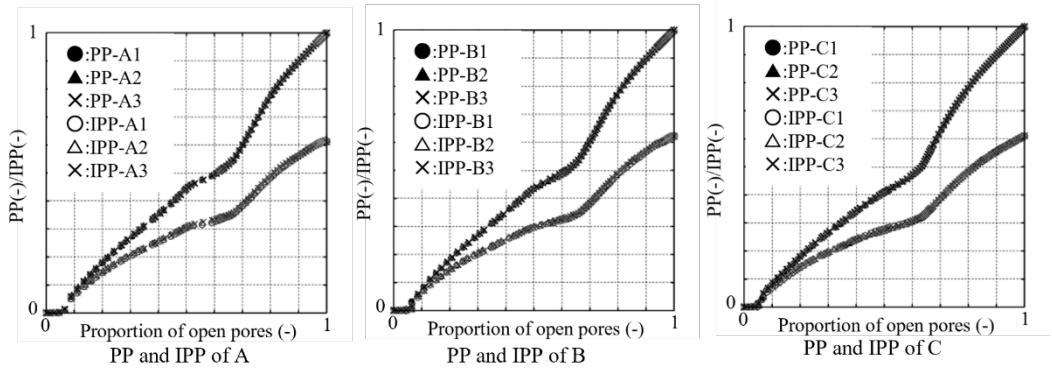

Fig. 12 Percolation probability (PP) and invaded percolation probability (IPP) of porous media with aggregates (Cases A, B and C: Pattern 2)

5. CONCLUSION

In this study, the spatial distribution and connectivity of pores in porous media with and without aggregate structures were investigated. Porous media with aggregate structures had larger Moran's *I* values than porous media without aggregate structures. This means there were larger cluster of similar sized pores in porous media with aggregate structure than media without aggregate. During the drainage process, the air entry pressure of the porous media with an aggregate structure was lower than that of the media without an aggregate structure. The percolation thresholds of both PP and IPP were lower in the porous media with aggregate structures than in the media without aggregate structures. This shows in porous media with aggregate structures fewer large pores formed subnetwork spread in whole media, and air started invading when fewer pores became invadable than in porous media without aggregate structures.

This study revealed that the graphs of the PP of porous media with an aggregate structure leave the diagonal in the middle and approach it again. This suggests that in the aggregate, mid-sized pores are surrounded by relatively small pores, and the former are loosely isolated from the larger pores. This contributes to the high water retention of soil with an aggregate structure.

In this study, pores of virtual porous media were investigated using pore network model. Pore network model has possibility to be applied to real porous media using X-ray computed microtomography images. The method used in this study could help to understand pore structure of real aggregate.

6. ACKNOWLEDGMENTS

This work was supported by JSPS KAKENHI Grant Number JP 20H03100.

7. REFERENCES

[1] Mangalassery S., S. Sjögersten, D. L. Sparkes, C. J. Sturrock, and S. J. Mooney, The Effect of Soil Aggregate Size on Pore Structure and Its Consequence on Emission of Greenhouse Gases, Soil and Tillage Research, Vol. 132, 2013, pp. 39-46.

[2] Wang H., S. Wang, R. Wang, Y. Zhang, and X. Wang, Direct and indirect linkages between soil aggregates and soil bacterial communities under tillage methods, Geoderma Vol. 354, 2019, p. 113879.

[3] Gao L., B. Wang, S. Li, H. Wu, X. Wu, G. Liang, D. Gong, X. Zhang, and A. D. Dianxiong Cai, Soil wet aggregate distribution and pore size distribution under different tillage systems after 16 years in the Loess Plateau of China, Catena Vol. 173, 2019, pp. 38-47.

[4] Zhou H., X. Peng, S. Peth, and T. Q. Xiao, Effects of Vegetation Restoration on Soil Aggregate Microstructure Quantified with Synchrotron-Based Micro-computed Tomography, Soil and Tillage Research, Vol. 124, 2012, pp. 17-23.

[5] Zhao D., M. Xu, G. Liu, L. Ma, S. Zhang, T. Xiao, and G. Peng, Effect of Vegetation Type on Microstructure of Soil Aggregates on the Loess Plateau, China, Agriculture, Ecosystems and Environment, Vol. 242, 2017, pp. 1-8.

[6] Wang W., A. N. Kravchenko, A. J. M. Smucker, W. Liang, and M. L. Rivers, Intra-aggregate Pore Characteristics: X-ray Computed Microtomography Analysis, Soil Science Society of America Journal, Vol. 76, Issue 4, 2012, pp. 1159-1171.

[7] Gao L., E. Becker, Guopeng Liang, A. A. Houssou, H. Wu, X. Wu, D. Cai, A. Degré, Effect of Different Tillage Systems on Aggregate Structure and Inner Distribution of Organic Carbon, Geoderma, Vol. 288, 2017, pp. 97-104.

[8] Peth S., R. Horn, F. Beckmann, T. Donath, J. Fischer, and A. J. M. Smucker, Three-Dimensional Quantification of Intra-aggregate Pore-Space Features Using Synchrotron-Radiation-Based Microtomography, Soil Science Society of America Journal, Vol. 72, Issue 4, 2008, pp. 897-907.

[9] Takeuchi J., Y. Song, Y. Takeuchi, and M. Fujihara, Spatial Statistics and Percolation Probability of Pore-Network in Porous Media with Aggregate Structure, in Proc. 12th Int. Conf. on GEOMATE, 2022, pp. 566-571.

[10] Coetzee C., A Johnson-Kendall-Roberts (JKR) Contact Model, Vol. 54404, 2020, p. 20, DOI:10.13140/RG.2.2.21772.

[11] Johnson K. L., K. Kendall, and A. D. Roberts, Surface Energy and the Contact of Elastic Solids, Proceedings of the Royal Society of London Series A – Mathematical and Physical Sciences, Vol. 324, Issue 1558, 1971, pp. 301-313.

[12] Gostick J. T., Versatile and Efficient Pore Network Extraction Method Using Marker-Based Watershed Segmentation, Physical Review. E, Vol. 96, Issue 2-1, 2017, p. 023307.

[13] Rabbani A., S. Jamshidi, and S. Salehi, An Automated Simple Algorithm for Realistic Pore Network Extraction from Micro-tomography Images, Journal of Petroleum Science and Engineering, Vol. 123, 2014, pp. 164-171.

[14] Okabe A. and K. Sugihara, Network Spatial autocorrelation, Spatial analysis along networks: Statistical and computational

methods, John Wiley & Sons, 2012, pp. 137-151.

[15] Takeuchi J. and M. Fujihara, Evaluation of Drainage Process in Porous Media by Invaded Percolation Probability, International Journal of GEOMATE, Vol. 17, Issue 59, 2019, pp. 90-97.

[16] Wilkinson D. and J. F. Willemsen, Invasion Percolation: A New Form of Percolation Theory, Journal of Physics. Part A: Mathematical and General, Vol. 16, Issue 14, 1983, pp. 3365-3376.

[17] Takeuchi J., W. Sumii, and M. Fujihara, Modeling of Fluid Intrusion into Porous Media with Mixed Wettabilities, International Journal of GEOMATE, Vol. 10, Issue 22, 2016, pp. 1971-1977.

[18] Takeuchi J., H. Tsuji, and M. Fujihara, Modeling of Permeability of Porous Media with Mixed Wettabilities Based on Noncircular Capillaries, International Journal of GEOMATE, Vol. 12, Issue 34, 2017, pp. 1-7.

[19] Takeuchi J. and M. Fujihara, Evaluation of Imbibition Process in Porous Media by Invaded Percolation Probability, International Journal of GEOMATE, Vol. 14, Issue 46, 2018, pp. 1-7.